Magalhäes, Regina, García-Ruiz, Andrés, Martins, Hugo F., Pereira, Joäo, Margulis, Walter, Martín-López, Sonia & González-Herráez, Miguel. 2019, "Fiber-based distributed Bolometry", Opt. Express, vol. 27, no. 4, pp. 4317-4328

Available at http://dx.doi.org/10.1364/OE.27.004317

Research Article | Vol. 27, No. 4 | 18 Feb 2019 | OPTICS EXPRESS 4317

Optics EXPRESS

Fiber-based distributed bolometry

REGINA MAGALHÃES,[1,*] ANDRES GARCIA-RUIZ,[1] HUGO F. MARTINS,[1] JOÃO PEREIRA,[2] WALTER MARGULIS,[2] SONIA MARTIN-LOPEZ,[1] AND MIGUEL GONZALEZ-HERRAEZ[1]

[1]*Dpto. de Electrónica, University of Alcalá, 28805, Alcalá de Henares (Madrid), Spain*
[2]*Acreo, Electrum 236, 16440, Stockholm, Sweden*
**regina.magalhaes@uah.es*

Abstract: Optical fibers are inherently designed to allow no interaction between the guided light and the surrounding optical radiation. Thus, very few optical fiber-based technologies exist in the field of optical radiation sensing. Accomplishing fully-distributed optical radiation sensing appears then as even more challenging since, on top of the lack of sensitivity explained above, we should add the need of addressing thousands of measurement points in a single, continuous optical cable. Nevertheless, it is clear that there exist a number of applications which could benefit from such a distributed sensing scheme, particularly if the sensitivity was sufficiently high to be able to measure correctly variations in optical radiation levels compatible with the earth surface. Distributed optical radiation sensing over large distances could be employed in applications such as Dynamic Line Rating (DLR), where it is known that solar radiation can be an important limiting factor in energy transmission through overhead power cables, and also in other applications such as thermo-solar energy. In this work, we present the proof-of-concept of the first distributed bolometer based on optical fiber technology and capable of detecting absolute changes of irradiance. The core idea of the system is the use of a special fiber coating with high emissivity (e.g., carbon coating or black paint). The high absorption of these coatings translates into a temperature change that can be read with sufficiently high sensitivity using phase-sensitive reflectometry. To demonstrate the concept, we interrogate distinct black-coated optical fibers using a chirped-pulse ΦOTDR, and we readily demonstrate the detection of light with resolutions in the order of 1% of the reference solar irradiance, offering a high-potential technology for integration in the aforementioned applications.

1. Introduction

Several engineering applications are currently seeking for measurement methods providing continuous distributed measurements of optical radiation over large distances, typically around a few tens of kilometers. One of the most interesting and promising applications for large-scale spatially-resolved optical radiation detection is the optimization of power transmission along overhead power lines [1]. The electrical line ratings are often kept below the optimum values, due to reliability and security concerns. A possible option to optimize the grid and improve efficiency is based on the concept of Dynamic Line Rating (DLR) [2]. DLR replaces the traditional static ratings by updating the ampacity values in real time based on weather conditions and cable temperature. In DLR, temperature acquisition over the cable is often combined with meteorological measurements, which allow for precise models of behavior of the line conductor and therefore optimal values of transmission line limits [3]. As recently reported [4], one of the environmental conditions that can considerably increase the temperature of the conductor in low wind speed conditions is solar radiation. Solar radiation has a direct influence in the ampacity of the conductor, and therefore should be monitored. However, very few dedicated technologies exist to enable this measurement in the power cable itself, and additionally, a single-point measurement of effective incident radiation is not

#349842 https://doi.org/10.1364/OE.27.004317
Journal © 2019 Received 2 Nov 2018; revised 20 Dec 2018; accepted 4 Jan 2019; published 6 Feb 2019

Optics EXPRESS

sufficient to fully characterize the global combined effect of solar irradiance along the whole span [4]. Therefore, there is a great interest in the dynamic and continuous monitoring of solar radiation along the conductor using distributed fiber sensing technology.

In other domains, Distributed Fiber Optic Sensors (DFOS) are gaining increasing attention due to their ability to perform continuous position-resolved measurements of different physical quantities along a certain monitored element. Distributed sensors allow replacing thousands of independent detectors which would be discretely disposed along a monitored structure or perimeter, by a single optical fiber cable connected to a single interrogation unit [5]. This way, DFOS allow for an increase in space and weight efficiency, and lead to a reduction in the overall complexity, energy consumption and cost-per-sensor of the monitoring system, particularly when large numbers of detectors are required. Thanks to this, DFOS have proven to be convenient and cost-effective solutions for several problems in engineering, being currently a standard monitoring tool in certain types of large infrastructures [6,7]. They have been shown to be particularly well-suited for the measurement of temperature [8–10], strain [11–13] and vibration/intrusions [14–19]. In the energy domain, they have been extensively used to monitor long-distance pipelines [20] and also hot spots in power lines, as a tool for preventing failures related to high-temperature degradation inside the conductors [21].

The core idea of optical fiber distributed sensing consists in exploiting scattering effects intrinsic to the optical fiber (in order to sense different physical variables) and localize such interaction by means of time or frequency-domain techniques. The scattering processes appearing in fibers are Rayleigh, Brillouin or Raman [22]. Since these phenomena are mostly temperature and/or strain dependent, DFOS are particularly well suited for the distributed measurement of these two physical quantities. Thus, distributed measurement of other parameters typically requires some type of transducing layer to convert the targeted physical quantity into a temperature or strain change in the fiber core. In the case of optical radiation, a possible solution might come by developing a photothermal-based distributed sensor, whose temperature changes in the presence of a certain irradiance. This could be accomplished by using a conventional optical fiber cable with a high emissivity coating. However, temperature resolutions of conventional distributed temperature sensors (e.g. Brillouin-based DFOS) are typically around 1 K [18]. With this low temperature resolution, this idea becomes impractical, as the amount of radiation needed to have a measurable change in the cable temperature would be too high. Considering the expected temperature increase experienced by the fiber due to the absorbed radiation at the earth surface, this would yield an approach with very poor sensitivity, and inconvenient for a practical use.

Recently, the use of linearly chirped pulses in phase-sensitive optical time domain reflectometry (CP-ΦOTDR) has allowed achieving fast (kHz), robust and high sensitivity (mK) distributed fiber temperature measurements over distances of up to 70 km [23,24]. With these sensitivities, the aforementioned ideas to develop a distributed bolometer are now made possible and practical. This is the starting point of our work. In this work, we make the proof-of-concept of the first distributed optical radiation sensor, operating as a distributed bolometer interrogated by a CP-ΦOTDR. To this end, we make use of black-coated fibers for increased absorption. The proposed method readily achieves a resolution compatible with solar radiation detection (≈1% of the reference solar spectral irradiance on earth [25]), achieving an important milestone in optical radiation sensing technology. This demonstration opens the door for important applications in industries related to solar radiation, creating a high-potential feasible solution which can be applied in different engineering sectors.

Optics EXPRESS

2. Principle of operation

2.1 Developing a bolometer

A bolometer can be implemented by connecting an absorptive element to a thermal reservoir with a constant temperature through a thermal link. Radiation reaching the absorber causes an increase in its temperature to a higher value than the reservoir temperature. Let us consider a heat sink with a temperature T_0, assumed constant, weakly connected to an absorptive element which has a temperature $T(\geq T_0)$. The temperature T depends on the incident irradiance reaching the absorber, E_{inc}. In the case of no incident radiation, $E_{inc} = 0$, then the temperature of the absorber will be equal to the temperature of the reservoir, $T = T_0$. When $E_{inc} > 0$, the absorber element absorbs an optical power $P_{abs} = E_{inc} \cdot A_{inc} \cdot \alpha$, which is proportional to the absorber area A_{inc}, and the absorption of the absorber, α. Consequently, T increases to a higher value than the heat sink temperature, so $T > T_0$. Assuming a small temperature difference $T - T_0$ between the elements, the absorber dissipates power to the heat sink, as described by Newton's law of cooling [24]:

$$P_{dissipated} = h \cdot A \cdot (T - T_0), \tag{1}$$

where h is the heat transfer coefficient between the absorber element and the reservoir, and A is the heat transfer surface area. The rate equation describing the balance of energy occurring in the bolometer system in these conditions is given by:

$$dE_{gained} - dE_{lost} = c \cdot m\, dT, \tag{2}$$

where c and m represent the absorber's specific heat and mass, respectively. The terms dE_{gained} and dE_{gained} are given by:

$$dE_{gained} = P_{abs}\, dt = E_{inc} \cdot A_{inc} \cdot \alpha\, dt \tag{3}$$

$$dE_{lost} = P_{dissipated}\, dt = h \cdot A \cdot (T - T_0)\, dt. \tag{4}$$

Therefore, the energy gained in the system depends on the optical power absorbed by the element, which increases for higher values of incident radiation, while the energy lost depends on the dissipated optical power to the reservoir. By replacing the previous relations in Eq. (2), we obtain:

$$E_{inc} \cdot A_{inc} \cdot \alpha\, dt - h \cdot A \cdot (T - T_0)\, dt = c \cdot m\, dT, \tag{5}$$

which, in a simpler way, can be described as:

$$\frac{dT}{dt} = bT - a, \tag{6}$$

being $a = -\frac{E_{inc} \cdot A_{inc} \cdot \alpha + h \cdot A \cdot T_0}{c \cdot m}$ and $b = -\frac{h \cdot A}{c \cdot m}$. The solution to this differential equation can be easily derived, and it has the form of:

$$T(t) = \frac{E_{inc} \cdot A_{inc} \cdot \alpha + h \cdot A \cdot T_0}{h \cdot A} + K \cdot \exp\left(\frac{-h \cdot A}{c \cdot m} t\right). \tag{7}$$

Considering that at $t = 0$ the temperature of the absorptive element is equal to the heat sink's temperature, $T(t = 0) = T_0$, we can calculate the value of the constant K, which is given by:

Optics EXPRESS

$$K = \frac{-E_{inc} \cdot A_{inc} \cdot \alpha}{h \cdot A}. \tag{8}$$

Finally, replacing the result from Eq. (8) in Eq. (7), we arrive to the general rate equation of the system which describes the temporal evolution of the element's temperature with relation to the applied irradiance:

$$T(t) = T_0 + \left(\frac{E_{inc} \cdot A_{inc} \cdot \alpha}{h \cdot A} \right) \cdot \left(1 - \exp\left(\frac{-h \cdot A}{c \cdot m} t \right) \right). \tag{9}$$

Furthermore, as it was seen from Eqs. (3) and (4), as the element's temperature increases due absorption, so does the dissipation, which is proportional to the difference in the temperatures between the element and the reservoir. Therefore, the system eventually evolves towards a thermal equilibrium state where $P_{abs} = P_{dissipated}$. Hence, by equaling $E_{inc} \cdot A_{inc} \cdot \alpha = h \cdot A \cdot (T - T_0)$, or simply by considering a large value of t in Eq. (9), it is derived the following relation at the thermal equilibrium state:

$$E_{inc} \simeq \frac{(T - T_0) \cdot (h \cdot A)}{(A_{inc} \cdot \alpha)} = \frac{(T - T_0)}{¢}, \tag{10}$$

where ¢ is a constant which depends on the system parameters. This way, given a certain system at the thermal equilibrium condition where all the necessary constants are known, the incident radiation E_{inc} can be calculated using the relation shown in Eq. (10).

2.2 Proposed fiber-based distributed bolometer

In this work, we recreate the bolometer operation principle using an optical fiber system. In the proposed configuration, a black-coated optical fiber is used as the absorbing element and the surrounding air is used as the heat sink, at T_0. A second fiber with much lower absorptance to the incident radiation (and hence different temperature) is connected to the same interrogation system. The temperature of both optical fibers is monitored with mK resolution using a CP-ΦOTDR, allowing for a highly accurate tracking of the temperature difference between both fibers. The proposed system can be analyzed considering that the two fibers present different absorptance values (α_1, α_2) to the incident radiation, and also (possibly) different heat transfer coefficients h_1, h_2. By monitoring the temperature difference between the two fibers simultaneously, it is possible to determine the value of irradiance reaching the fibers. In this case, the equilibrium state with the surrounding air will be reached at different temperatures, T_1, T_2, for the fibers *1* and *2*:

$$E_{inc} = \frac{(T_1 - T_0) \cdot (h_1 \cdot A)}{A_{inc} \cdot \alpha_1} = \frac{(T_1 - T_0)}{¢_1} \Leftrightarrow T_0 = T_1 - (E_{inc} \cdot ¢_1) \tag{11}$$

$$E_{inc} = \frac{(T_2 - T_0) \cdot (h_2 \cdot A)}{A_{inc} \cdot \alpha_2} = \frac{(T_2 - T_0)}{¢_2} \Leftrightarrow T_0 = T_2 - (E_{inc} \cdot ¢_2). \tag{12}$$

By replacing Eq. (11) in Eq. (12), it is then derived that:

$$E_{inc} = \frac{(T_2 - T_1)}{(¢_2 - ¢_1)}. \tag{13}$$

This way, by using two fibers with different coating (and therefore distinct optical absorption coefficients), an incident irradiance E_{inc} can be measured given an unknown external temperature value, T_0, by simply measuring the difference between the temperature shifts

Optics EXPRESS

obtained for the two fibers. Additionally, the values of ¢1 and ¢2 can also accommodate for different values of the heat transfer coefficient h and are not really needed individually, but only the value of the difference $¢_2 - ¢_1$. This can easily be obtained by applying a known E_{inc} to the reference and the absorber fiber, and by measuring the resulting $T_2 - T_1$ in equilibrium.

3. Experimental setup

3.1 CP-ϕOTDR: Distributed temperature sensor

The experimental setup proposed for the proof-of-concept demonstration of a distributed bolometer is depicted in Fig. 1. A CP-ΦOTDR interrogator [23] was used to monitor the temperature of the reference and the absorber optical fibers. This monitoring tool allows for high sensitivity and fast distributed measurements of temperature variations. Further information on the operation of this measurement technique can be found in [23].

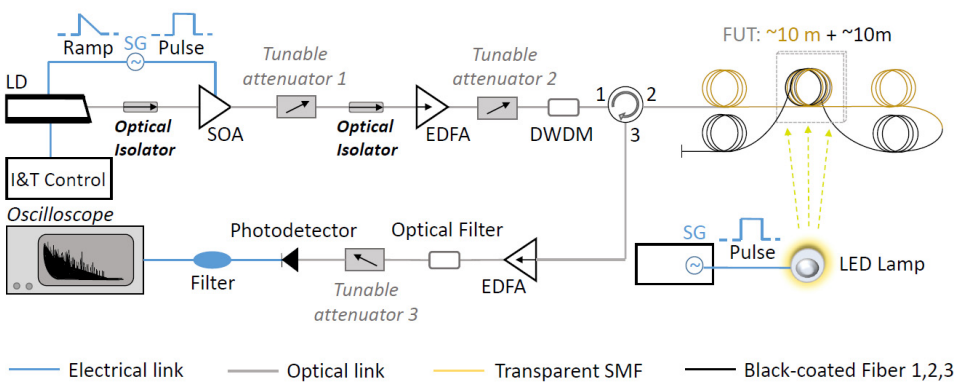

Fig. 1. Experimental setup: acronyms are explained in the text.

The specific interrogation scheme used in this work is very similar to the one used in one of our former works [24]. It consists of a block responsible for generating linearly-chirped pulses and sending them towards the Fibers Under Test (FUTs); and a second block responsible for the detection of the Rayleigh backscattered light generated during the process. To generate the linearly-chirped pulses, a Laser Diode (LD) working in continuous emission, driven by a standard temperature and current controller (I&T), was modulated in current through an electrical ramp signal from a Signal Generator (SG). By synchronizing the laser current modulation with a square-wave to the driver of a Semiconductor Optical Amplifier (SOA), linearly-chirped pulses could be formed. The pulses were then amplified by means of an Erbium-doped Fiber Amplifier (EDFA). The pulse power was controlled with a tunable attenuator in order to prevent the advent of non-linear effects in the optical fiber, and filtered using a Dense Wavelength-division Multiplexer (DWDM) to reduce the amplified spontaneous emission (ASE) produced by the amplifier. The pulses were launched into the FUTs through an optical circulator. The generated Rayleigh backscattered light was then collected, amplified and filtered before reaching the photodetector, after which it was recorded by a high-speed digitizer.

In this case, the CP-ΦOTDR measurements were performed using 100 ns pulses, corresponding to a 10-meter spatial resolution. These pulses were linearly chirped with ≈1 GHz of total pulse frequency content. The detection scheme enables a temperature sampling period of 40 ms, resulting in a temperature resolution of ≈2 mK. Although a simple proof-of-concept of a distributed bolometer is intended in this work, this method could be readily extended to match the limits set by the interrogation technique (CP-ΦOTDR), which could reach mK resolutions over up to 70 km, with metric spatial resolution and sampling rates in

Optics EXPRESS

the order of 1 kHz [23]. A more detailed description of the FUTs interrogated with this method is found in section 3.3.

3.2 Fiber-based bolometer system

In Fig. 2, a more detailed representation of the irradiance detection part of the setup is presented. It refers to the optical radiation emission/absorption mechanism, which can be found after the optical circulator in Fig. 1. As mentioned above, the distributed bolometer system consists in monitoring the temperature difference between two standard fibers with different coatings (and thus, different absorption coefficients). Therefore, a normal transparent-coating single-mode fiber (lower absorption coefficient) was used as the temperature reference fiber, FUT_1. Three distinct black-coated fibers with higher absorption coefficients were tested as the absorptive-sensitive fiber, FUT_2. All the FUTs had an outer diameter of ~0.25 mm, and each FUT had an overlapping section of ~10 m, corresponding to the interrogator spatial resolution. The ~10m of the reference FUT_1 and of each absorbing FUT_2 were wrapped in concentric circles with a radius of ~10 cm. They were placed contiguous to each other with the transparent fiber in front, as shown in Fig. 2. This ensured that both fibers experienced the same environmental conditions and that they received the same uniform radiation along, at least, the length of the interrogator spatial resolution. The two optical fibers were spliced together, so that they could be simultaneously monitored by the CP-ΦOTDR interrogator.

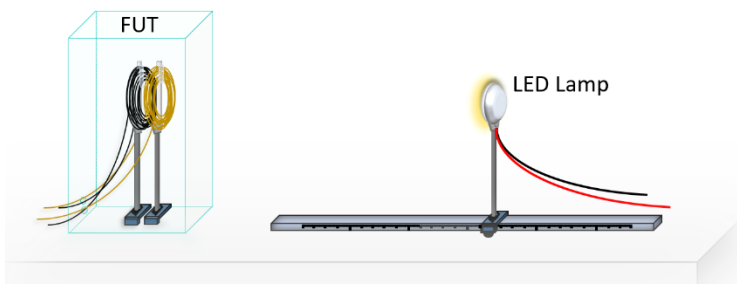

Fig. 2. Representation of the optical radiation emission/absorption mechanism.

A warm white LED lamp, operating at 12 V with 800-1000 total lumens, was used as optical radiation source emitting visible radiation towards the fibers. The lamp was disposed on a translation stage, enabling it to move and to be placed at difference discrete positions. This way, by changing the distance between the optical radiation source and the FUTs, different irradiance values could be applied to the fibers. The applied irradiance values were also monitored by a calibrated optical radiometer placed at the FUTs position.

3.3 Absorptive optical fibers

As it was mentioned above, different black-coated fibers were interrogated using the proposed method, in order to study the temperature response obtained under different absorption conditions. One of the highly-absorptive optical fibers tested was simply a black-painted fiber, which consists of a normal SMF with the coating dyed in black. The layer of black dye is estimated to be ~40 µm thick, giving the fiber a total coating thickness of ~102.5 µm. A multi-mode and a single-mode carbon-coated fibers were also interrogated [26]. These have a ~20 nm thick carbon film deposited between the glass surface and the primary coating, and were used since, in addition of having a dark-coating (i.e. high absorptance to the incident radiation) as seen in Fig. 3, they are widely industrialized fibers, which means that they can offer a reliable and feasible solution for a ready implementation. The single-mode carbon-coated fiber used in these tests has an acrylate primary coating with a thickness of 62.5 µm, while the multi-mode carbon-coated fiber includes a polyimide primary coating with a

Optics EXPRESS

thickness of 20 μm. The acrylate gives to the single-mode carbon fiber a silver shine on the top of the dark color, while the polyimide is responsible for a dark yellow color in the multi-mode fiber. The three aforementioned fibers were used to demonstrate the principle of operation shown above, and were also tested under dynamic irradiance measurements.

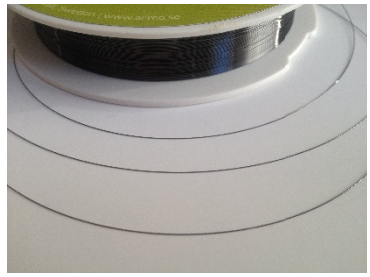

Fig. 3. Example of a carbon-coated optical fiber employed in the proposed setup.

4. Results

4.1 Proof-of-concept

In the proof-of-concept demonstration the fibers were characterized under long cycles of irradiance, in order to approximate the experiment to a thermal equilibrium state. They were studied under five irradiance values chosen to simulate field conditions, which were applied in cycles of 25 s or 35 s each (depending on the saturation regime of the fiber). The sequence of irradiance values applied to all the FUTs was: (1) E_{inc} = 0 W/m^2 (LED turned off), (2) E_{inc} = 43.8 W/m^2, (3) E_{inc} = 30.3 W/m^2, (4) E_{inc} = 14.8 W/m^2, (5) E_{inc} = 0 W/m^2 (LED turned off). Note that all FUTs had a cross section area of ≈0.0025 m^2 over 10 m of fiber length, meaning that the radiation power reaching the fibers varied between 0 mW up to 110 mW. The results obtained can be observed in Figs. 4(a), 5(a) and 6(a), regarding the temperature shifts experienced by the multi-mode carbon-coated, single-mode carbon-coated, and black-painted fiber, respectively. The temperature calibration obtained by the difference between the two FUT's temperature shifted signals is shown in Figs. 4(b), 5(b) and 6(b), accordingly.

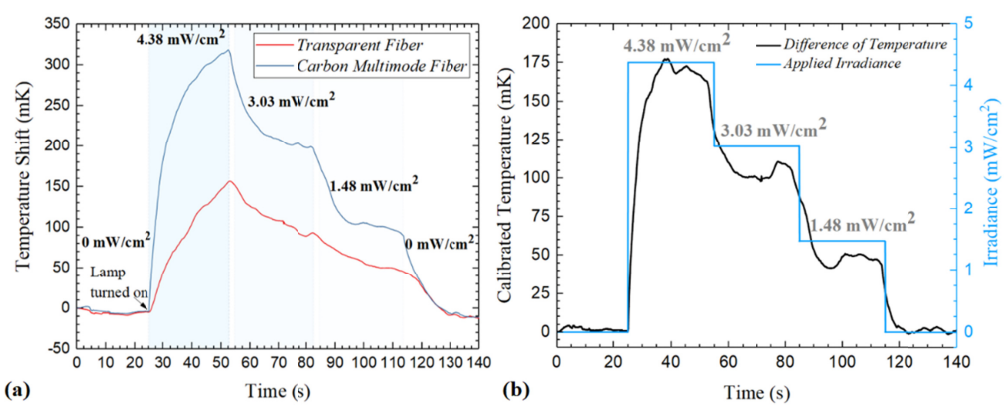

Fig. 4. **(a) -** Temperature shift experienced by the reference fiber, FUT$_1$ (red line), and by the carbon-coated multi-mode FUT$_2$ (blue line), when submitted to irradiances of I ≈43.8 W/m^2, II ≈30.3 W/m^2 and III ≈14.8 W/m^2, at room temperature. **(b) –** Difference between the FUT's temperature shifted signals (temperature calibration), vs the applied irradiance.

Optics EXPRESS

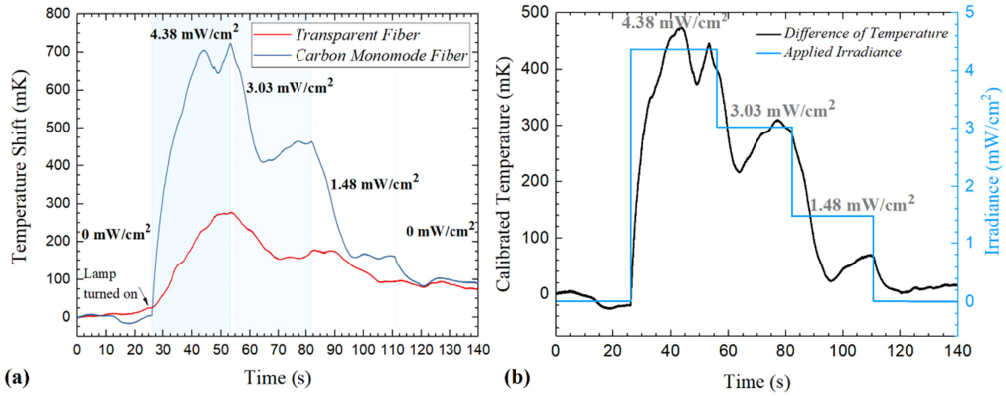

Fig. 5. **(a)** - Temperature shift experienced by the reference fiber, FUT1 (red line), and by the carbon-coated single-mode FUT2 (blue line), when submitted to irradiances of I ≈43.8 W/m^2, II ≈30.3 W/m^2 and III ≈14.8 W/m^2, at room temperature. **(b)** – Difference between the FUT's temperature shifted signals (temperature calibration), vs the applied irradiance.

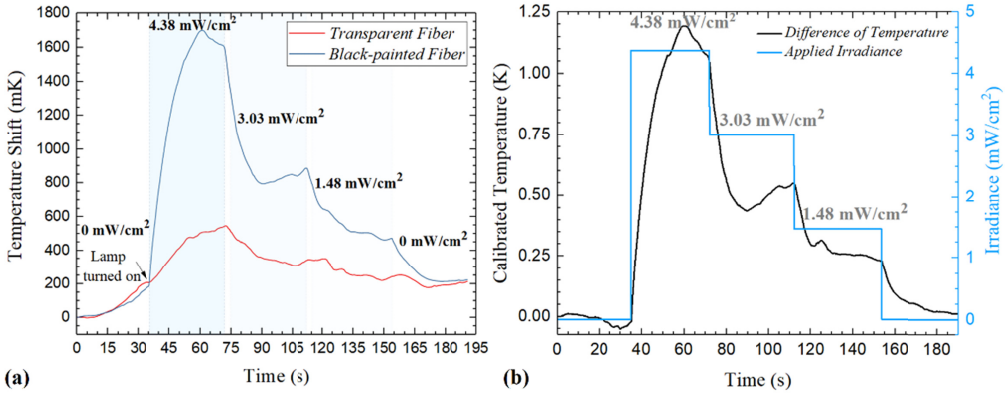

Fig. 6. **(a)** - Temperature shift experienced by the reference fiber, FUT1 (red line), and by the black-painted single-mode FUT2 (blue line), when submitted to irradiances of I ≈43.8 W/m^2, II ≈30.3 W/m^2 and III ≈14.8 W/m^2, at room temperature. **(b)** – Difference between the FUT's temperature shifted signals (temperature calibration), vs the applied irradiance.

A clear demonstration of the fiber-based distributed bolometry operation principle is obtained from the results presented in Figs. 4-6. A temperature difference between FUT_1 and all the $FUTs_2$ is measured, a difference which changes under different irradiance values. This behavior was already expected from Eq. (13), considering the different absorption coefficients and features of the fibers. From the attained results (and considering Eq. (13)), a value of 1/(¢2-¢1) ≈250 (Wm^{-2}K^{-1}) can be estimated considering the multi-mode carbon-coated fiber results. Regarding the single-mode fibers, a value of 1/(¢2-¢1) ≈100 (Wm^{-2}K^{-1}) was achieved for the single-mode carbon-coated fiber, and of 1/(¢2-¢1) ≈40 (Wm^{-2}K^{-1}) for the black-painted fiber. These results indicate that the black-painted fiber offers a greater sensitivity to irradiance measurements, and therefore a higher absorption, when compared to the other two. This is caused by the darker color of the coating when comparing to carbon-coated fibers, and also by a larger coating thickness along the fiber. A difference between the sensitivities of the carbon-coated fibers was also observed, related to the fact that the single-mode fiber presents a larger thickness and a different coating material when compared to the multi-mode fiber. While the multi-mode fiber has a coating thickness of 20 µm, the single-mode fiber has a larger coating thickness of 62.5 µm, presenting a higher sensitivity of more than twice than the multi-mode carbon fiber. Considering the carbon-coated fibers, we also

Optics EXPRESS

verified as well that the experimentally obtained value of α/h was within the range of expectable theoretical values (according to the large variability of α and h). Also note that the sensitivity of one of the carbon fibers was characterized at three different positions, obtaining an equal sensitivity within the error of our measuring system. This indicates that we can rely on a constant sensitivity of the carbon-coated fibers along its length, as it was expected. Anyway, a reasonable sensitivity was achieved with the industrially fabricated fibers, in particular with the single-mode carbon-coated fiber, showing that this sensor can potentially be used in long distance applications. However, the ratio between applied radiances and temperature shifts for each set of fibers should be constant. The error in the measurements can have occurred since the temperature signals do not reach a perfect equilibrium state in the short cycles between irradiance stages (3.33 to 10 seconds). In any case, note that the step between the irradiances applied (≈15 W/m^2) corresponds to only ≈1.5% of the reference solar spectral irradiance on earth at surface level [25]. This is an important result, since it demonstrates the compatibility between our proposed method and real solar-based applications.

4.2 Dynamic optical radiation measurements

After demonstrating the working principle, dynamic measurements were performed to the fibers in the transient-regime, in order to characterize the system linearity. Instead of using only one cycle of 25s or 35s for each given irradiance, the fibers were characterized without reaching the thermal equilibrium. They were interrogated under shorter irradiance cycles of 10s, 5s and 3.33 s, periodically applied over several minutes. The driving motivation behind this method is that by computing enough short cycles in a sufficiently long measurement (considering the time of temperature drifts), the amplitude of the signal obtained by a Fourier transform already compensates for the external fluctuations occurring during the measurements. Also, this amplitude provides a measurement which is proportional to the absorption coefficient of the fiber. This way, the use of a second fiber is not necessary, and it is also possible to characterize the absorption coefficients (α in Eq. (7)) of individual fibers separately.

Therefore, the dynamic optical radiation was applied using a square wave at the LED electrical input. This results in alternating “on” and “off” states of the lamp, with a specific amplitude. The distinct values of irradiance were applied by moving the lamp with the translation stage, and they were applied to the absorptive fibers, being the reference temperature fiber removed. Since thermal equilibrium is never reached along the multiple cycles, the fiber temperature oscillates around a certain mean value. The amplitude of these temperature oscillations is expected to be linearly proportional to the amplitude of the applied irradiance, as it is proportional to the absorbed optical power ($P_{abs} = E_{inc} \cdot A_{inc} \cdot \alpha$, see Introduction). Or, in a different way, the linearity can be expected from the rate equation outside equilibrium (Eq. (9)), considering the same time for each incident irradiance at the absorber.

Figure 7 shows the results obtained for the amplitude of the temperature sensor regarding the different applied irradiances, using three square wave signals with periods of 10 s, 5 s and 3.33 s. Once again, a higher sensitivity was achieved using the black-painted fiber, followed by the single-mode carbon-coated fiber. These results are in agreement with the ones obtained in the previous section, which are directly linked to the absorption coefficient values of each structure. All tested fibers showed a linear amplitude response to the applied irradiance, as expected. The amplitude of the temperature oscillations depends on the period of the applied square function, since for larger periodic cycles the fiber will undergo a larger exposure time, increasing, therefore, the absorbed optical power (and also the time to cool down, so it starts again from a lower value). The different slopes obtained for each fiber were expected from Eq. (9), since for a certain fixed value of irradiance, the linear relation between the

Optics EXPRESS

temperature and the incident irradiance should follow a greater slope for higher exposition times, according to the expression.

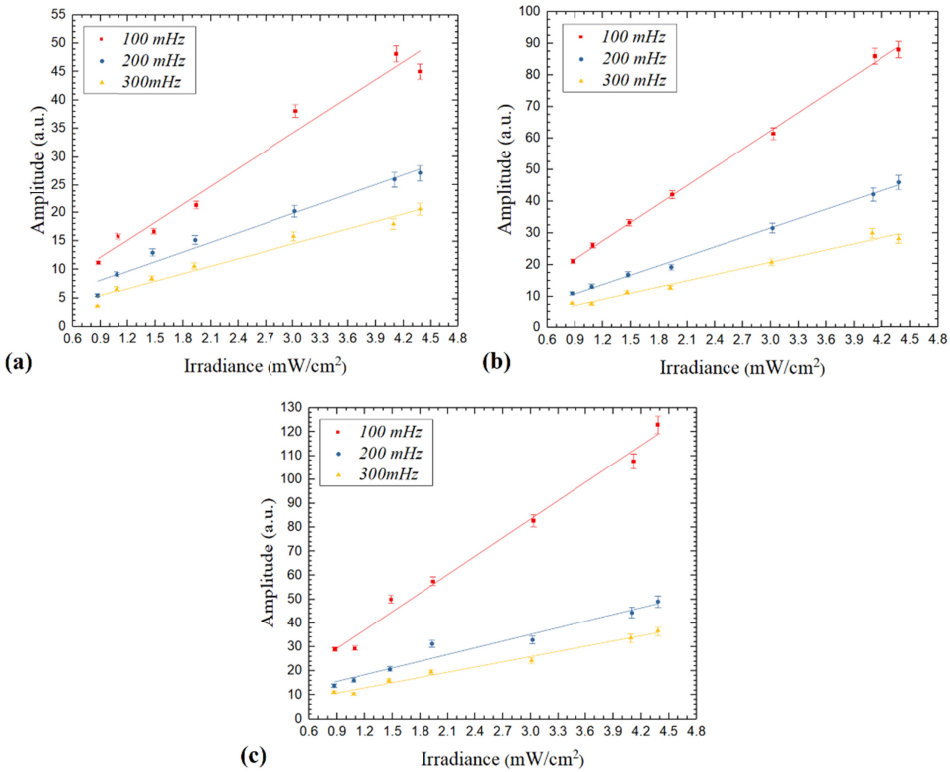

Fig. 7. Amplitude of the temperature sensor oscillations vs the applied Irradiance, which was applied through a square wave with the periods of 10, 5 and 3.33 s. Results attained for the (a) – multi-mode carbon-coated fiber, (b) single-mode carbon-coated fiber and (c) - black-painted single-mode fiber.

It should be noted that the approach of dynamic assessment of the optical fibers allows for measurements immune to offsets / small drifts of the temperature of the surrounding air, as the mean value of the temperature oscillations is not crucial, making this a robust procedure for fiber characterization to be used in certain conditions where a modulated light source could be employed. Ultimately, with the existence of strong temperature drifts (comparable to the dynamic temperature variations) the system would not reach thermal equilibrium (where a repeatable temperature variation cycle around a constant average temperature occurs), and the temperature variations would be composed of two contributions: the repeatable temperature cycle (to be measured), and the temperature drift of the system tending to the average temperature in equilibrium. In this case, an offset would be added to the linear plots of Figs. 7(a)-7(c), since this temperature drift would also have its own spectral power function. In any case, in the presented measurements such an effect is either not existent or negligible (the linear fits almost cross zero, within the measurement error), which demonstrates the robustness of the system.

5. Conclusions

In this work, a proof-of-concept demonstration of the first fiber-based distributed bolometer was presented. The method is based on using two fibers with coatings showing different absorptance to the incident radiation. By sensitively measuring the temperature difference between the two optical fibers, it is possible to demonstrate the detection of absolute values of

Optics EXPRESS

irradiance without knowledge of the surrounding temperature. The interrogation technique used (CP-ΦOTDR) enabled high-sensitivity measurements of this temperature difference, while enabling to monitor tens of km-long distances in a spatially continuous fashion. Three different optical fibers were interrogated, showing that the proposed method is sufficiently sensitive using both multi-mode and single-mode fibers, showing a slightly increased sensitivity in the single-mode case. Employing a black-painted single-mode fiber (with higher emissivity and a slightly thicker coating) endows greater sensitivity in the optical irradiance absorption when compared to the other tested coatings, though new and/or existing enhanced fiber-coatings may as well be tested with this method. The sensor was readily demonstrated to be able to measure absolute values of irradiance with sensitivities of the order of 10 W/m^2 (equivalent to ≈1% of the reference solar spectral irradiance at the earth surface), and corresponding to temperature differences of ≈150 mK. However, the available sensitivities with the CP-ΦOTDR can reach ~2mK over tens of km with meter scale spatial resolutions. Therefore, the proposed sensor can be further explored in order to match its full capability.

Overall, the demonstrated detector has a high potential for integration in solar radiation-based applications, such as DLR forecasting or photovoltaic industries, becoming the first but feasible solution in distributed fiber-based optical radiation sensing. In this sense, the presented photothermal optical radiation sensor has been proven to work with already industrially available fibers, offering a reliable and ready-to-implement solution. Considering that the interrogated quantity is the temperature, the proposed system also provides the possibility of working at conventional telecom wavelengths, being feasible to integrate using conventional communication components. To approach practical applications, it is necessary to assess the operation of this method at a real time-scale. Further studies should be developed evaluating the response of the sensor in a 24h time-scale evaluation, in order to demonstrate the compatibility with real daily solar irradiance values along a whole day. Nevertheless, considering the average irradiance change along a full day and the sensitivity of our system (1% of the irradiance reference), this method should be compliant with those standards. Other experimental conditions should as well be improved in future studies in order to better approach the applied irradiation to normal solar conditions, as for example the integration of a lamp whose features are closer to solar irradiation and farther from the blue-emission zone.

Lastly, it could also be envisaged that optical fibers with different coating-colors might also be interrogated by CP-ΦOTDR, in order to achieve a spectral footprint associated with each fiber color and more advanced distributed bolometry based on spectral discrimination.

Funding

H2020 European Research Council through project U FINE (307441); European Commission (MSCA-ITN-ETN-722509); DOMINO Water JPI project, under the WaterWorks2014 cofounded call by Horizon 2020 Framework Programme (European Union) and Ministerio de Economía y Competitividad, Spain; Ministerio de Economía y Competitividad, Spain (TEC2015-71127-C2-2-R, "Ramón y Cajal" contract); Sensores e INstrumentación en tecnologías FOTÓNicas (S2013/MIT-2790).

Acknowledgments

The work of RM and JP was supported by European Commission funding through the project FINESSE MSCA-ITN-ETN-722509. The work of SML was supported by the Ministerio de Economía y Competitividad, Spain, through a "Ramón y Cajal" contract.

References

1. Y. Yang, D. Divan, R. G. Harley, and T. G. Habetler, "Power line sensornet - a new concept for power grid monitoring," in Power Eng. Soc. General Meeting, (IEEE, 2006).
2. D. Douglass, W. Chisholm, G. Davidson, I. Grant, K. Lindsey, M. Lancaster, D. Lawry, T. McCarthy, C. Nascimento, M. Pasha, J. Reding, T. Seppa, J. Toth, and P. Waltz, "Real-time overhead transmission-line monitoring for dynamic rating," IEEE Trans. Power Deliv. **31**(3), 921–927 (2016).

Optics EXPRESS

3. S. Karimi, P. Musilek, and A. M. Knight, "Dynamic thermal rating of transmission lines: A review," Renew. Sustain. Energy Rev. **91**, 600–612 (2018).
4. A. Michiorri, H. Nguyen, S. Alessandrini, J. B. Bremnes, S. Dierer, E. Ferrero, B. Nygaard, P. Pinson, N. Thomaidis, and S. Uski, "Forecasting for dynamic line rating," Renew. Sustain. Energy Rev. **52**, 1713–1730 (2015).
5. D. Inaudi and B. Glisic, "Long-range pipeline monitoring by distributed fiber optic sensing," J. Press. Vessel Technol. **132**(1), 011701 (2010).
6. X. Bao and L. Chen, "Recent progress in distributed fiber optic sensors," Sensors (Basel) **12**(7), 8601–8639 (2012).
7. G. Yilmaz and S. E. Karlik, "A distributed optical fiber sensor for temperature detection in power cables," Sensor Actuat. A. Phys. **125**(2), 148–155 (2006).
8. G. Bolognini, J. Park, M. A. Soto, N. Park, and F. Di Pasquale, "Analysis of distributed temperature sensing based on Raman scattering using OTDR coding and discrete Raman amplification," Meas. Sci. Technol. **18**(10), 3211–3218 (2007).
9. M. A. Soto, T. Nannipieri, A. Signorini, A. Lazzeri, F. Baronti, R. Roncella, G. Bolognini, and F. Di Pasquale, "Raman-based distributed temperature sensor with 1 m spatial resolution over 26 km SMF using low-repetition-rate cyclic pulse coding," Opt. Lett. **36**(13), 2557–2559 (2011).
10. X. Angulo-Vinuesa, S. Martin-Lopez, J. Nuño, P. Corredera, J. D. Ania-Castañon, L. Thévenaz, and M. Gonzalez-Herraez, "Raman-assisted brillouin distributed temperature sensor over 100 km featuring 2 m resolution and 1.2°C uncertainty," J. Lightwave Technol. **30**(8), 1060–1065 (2012).
11. S. Le Floch, F. Sauser, M. A. Soto, and L. Thévenaz, "Time/frequency coding for Brillouin distributed sensors," Proc. SPIE **8421**, 84211J (2012).
12. M. A. Soto, G. Bolognini, and F. Di Pasquale, "Analysis of pulse modulation format in coded BOTDA sensors," Opt. Express **18**(14), 14878–14892 (2010).
13. M. A. Soto, G. Bolognini, F. Di Pasquale, and L. Thévenaz, "Simplex-coded BOTDA fiber sensor with 1 m spatial resolution over a 50 km range," Opt. Lett. **35**(2), 259–261 (2010).
14. J. C. Juarez, E. W. Maier, K. N. Choi, and H. F. Taylor, "Distributed fiber-optic intrusion sensor system," J. Lightwave Technol. **23**(6), 2081–2087 (2005).
15. H. F. Martins, S. Martin-Lopez, P. Corredera, M. L. Filograno, O. Frazão, and M. González-Herráez, "Coherent noise reduction in high visibility phase-sensitive optical time domain reflectometer for distributed sensing of ultrasonic waves," J. Lightwave Technol. **31**(23), 3631–3637 (2013).
16. Z. Qin, L. Chen, and X. Bao, "Wavelet denoising method for improving detection performance of distributed vibration sensor," IEEE Photonics Technol. Lett. **24**(7), 542–544 (2012).
17. L. B. Liokumovich, N. A. Ushakov, O. I. Kotov, M. A. Bisyarin, and A. H. Hartog, "Fundamentals of optical fiber sensing schemes based on coherent optical time domain reflectometry: signal model under static fiber conditions," J. Lightwave Technol. **33**(17), 3660–3671 (2015).
18. Y. Koyamada, M. Imahama, K. Kubota, and K. Hogari, "Fiber-optic distributed strain and temperature sensing with very high measurand resolution over long range using coherent OTDR," J. Lightwave Technol. **27**(9), 1142–1146 (2009).
19. H. F. Martins, S. Martin-Lopez, P. Corredera, M. L. Filograno, O. Frazão, and M. Gonzalez-Herraez, "Phase-sensitive optical time domain reflectometer assisted by first-order Raman amplification for distributed vibration sensing over >100km," J. Lightwave Technol. **32**(8), 1510–1518 (2014).
20. F. Tanimola and D. Hill, "Distributed fibre optic sensors for pipeline protection," J. Nat. Gas Sci. Eng. **1**(4–5), 134–143 (2009).
21. A. Ukil, H. Braendle, and P. Krippner, "Distributed temperature sensing: review of technology and applications," IEEE Sens. J. **12**(5), 885–892 (2012).
22. A. D. Kersey, "A review of recent developments in fiber optic sensor technology," Opt. Fiber Technol. **2**(3), 291–317 (1996).
23. J. Pastor-Graells, H. F. Martins, A. Garcia-Ruiz, S. Martin-Lopez, and M. Gonzalez-Herraez, "Single-shot distributed temperature and strain tracking using direct detection phase-sensitive OTDR with chirped pulses," Opt. Express **24**(12), 13121–13133 (2016).
24. A. Garcia-Ruiz, J. Pastor-Graells, H. F. Martins, K. H. Tow, L. Thévenaz, S. Martin-Lopez, and M. Gonzalez-Herraez, "Distributed photothermal spectroscopy in microstructured optical fibers: towards high-resolution mapping of gas presence over long distances," Opt. Express **25**(3), 1789–1805 (2017).
25. ASTM, "Standard tables for reference solar spectral irradiances: direct normal and hemispherical on 37° tilted surface," **14**(4), (2012).
26. A. Sudirman, L. Norin, and W. Margulis, "Increased sensitivity in fiber-based spectroscopy using carbon-coated fiber," Opt. Express **20**(27), 28049–28055 (2012).